Intraplate Earthquakes in Europe—Source Parameters from Regional Moment Tensor Analysis

Jochen Braunmiller

1 Introduction

Plate tectonics provides a highly successful framework to describe a wide range of geological observations invoking the motion of lithospheric plates. In its simplest form the plates are rigid and earthquakes are confined to boundaries where plates move relative to each other. Over 90% of all earthquakes (Johnston 1989) follow this tenet and, considering that subduction zone earthquakes are the largest seismic events, an even higher percentage of the global seismic moment is released along plate boundaries. However, plate interiors are not entirely aseismic and experience rare, large earthquakes such as the 1811–1812 New Madrid earthquakes (e.g., Johnston 1996). Causes for intraplate earthquakes are debated but probably involve transfer of stresses exerted at plate boundaries to plate interiors with seismicity seemingly concentrated along zones of preexisting weakness (e.g., Stein and Mazzotti (2007) and Talwani (2014) for overviews on intraplate earthquakes).

Seismicity in the European-Mediterranean region follows the plate boundary zones (Fig. 1) related to the convergence of the Africa (Nubia), Adria, and Arabia plates relative to Eurasia. A significant number of earthquakes, however, are located inside the Eurasian plate. The earthquakes considered here include events in the stable continental region (SCR) of northern and central-western Europe (blue and brown shading in Fig. 1) as well as events in broad, actively deforming regions such as the Hellenic backarc and the Caucasus Arabia-Eurasia collision zone (yellow in Fig. 1). SCRs, as defined in Johnston et al. (1994), are areas of continental crust with no major tectonic, magmatic, basement metamorphic or anorogenic intrusive event since the early Cretaceous and no other major extension, rifting or transtension event since the Paleogene. Shading in Fig. 1 indicates regions experiencing the last major tectonic event in the Precambrian (brown), Paleozoic (blue), and Mesozoic (yellow)

J. Braunmiller (✉)
School of Geosciences, University of South Florida, Tampa, FL 33620, USA
e-mail: jbraunmiller@usf.edu

S. D'Amico (ed.), *Moment Tensor Solutions*, Springer Natural Hazards,
https://doi.org/10.1007/978-3-319-77359-9_15

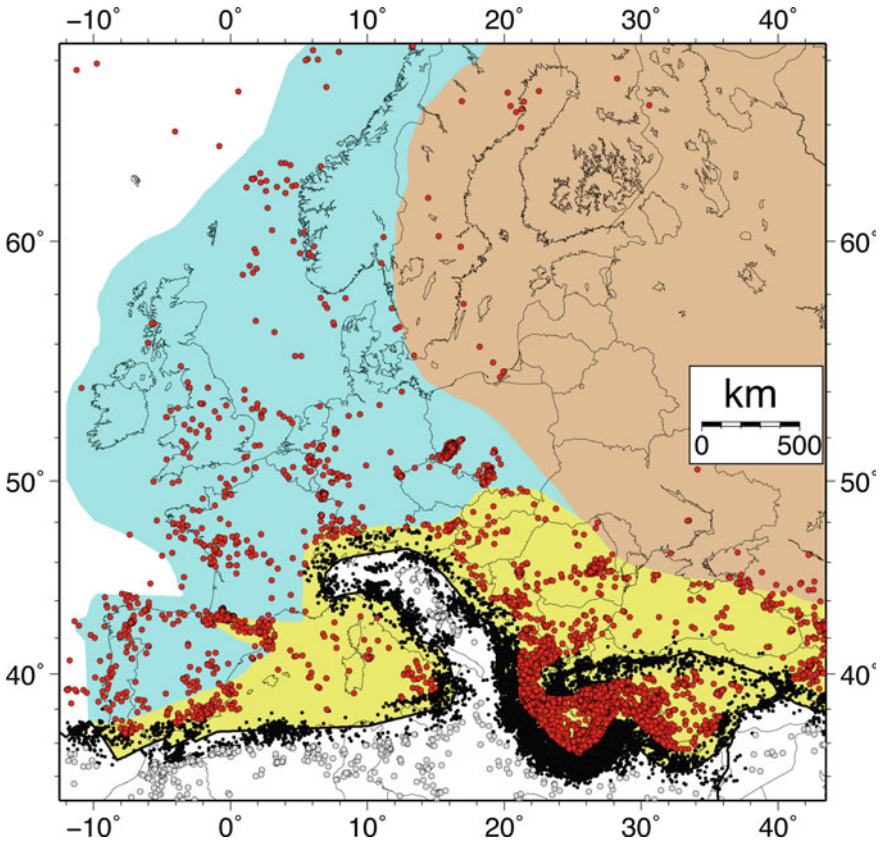

Fig. 1 Seismicity in Europe. Shown are 23,100+ magnitude M ≥ 3.5 earthquakes from the USGS PDE catalog from 1989 to June 2016 (27.5 years). Red, gray: Intraplate earthquakes (taken as ≥ 125 km from plate boundary) in Eurasia and other plates, respectively. Black: plate boundary events. Solid black lines are plate boundaries from the PLATES Project (Coffin et al. 1998) and extended to include the Adria microplate. Brown, blue, and yellow shading for regions experiencing last major tectonic phase in the Precambrian, Paleozoic, and Mesozoic era, respectively, after Johnston et al. (1994)

eras, respectively, following maps in Johnston et al. (1994). In Western Europe, I include earthquakes within ~50 km of the Paleozoic-Mesozoic boundary to the SCR dataset, but also show results excluding these events.

The systematic retrieval of earthquake source parameters may improve the understanding of causes for intraplate seismicity, for example, in relation to acting stresses and existing geologic structures. However, seismicity away from broad deforming plate boundary zones is low (Fig. 1) and larger events (moment magnitude M_w 5.0 and more) that can be analyzed with teleseismic waveforms occur infrequently. The broadband seismic networks in Europe, which started to be installed in the 1990s, offer an opportunity to obtain moment tensors for the more frequent moderate-sized

events ($M_w \geq 4.0$–4.5). Here, I combine robust and reliable regional moment tensor (for 1995–2007) and Global CMT (for 1976–2015) databases to investigate deformation style, stress field orientation, and depth distribution of crustal intraplate earthquakes in Europe with focus on its SCR part.

2 Seismicity

Seismicity inside the European plate is considerably lower than at its plate boundaries and large intraplate events are rare. Figure 1 shows 27.5 years (1989-June 2016) of seismicity with magnitude $M \geq 3.5$ from the USGS PDE catalog. More than 68% of the 23,100+ events occurred along plate boundaries (black in Fig. 1) and another 20% occurred in the broadly deforming Aegean and western Anatolia regions, the Caucasus and the Vrancea zone, Romania (red circles in Fig. 1 east of 20° E and south of 46° N). Less than 6% of seismicity occurred in the rest of Europe (remaining red circles in Fig. 1). For simplicity, I will refer to earthquakes in this latter region as "intraplate" in contrast to events in the broad plate boundary zone in the larger Aegean-Anatolian region. (The rest are events in northern Africa, Arabia, and Adriatic—2%—and mining related events in southwest Poland—4%).

The Precambrian shield region (brown shading) with only about 1 $M \geq 3.5$ event per year is essentially aseismic away from its exterior boundaries. Seismicity rate in the Paleozoic (blue) and the western Mesozoic (yellow, west of 20° E) parts of Europe are similar and combine to about 50 events per year. Seismicity shows clear areas of concentration that are separated from relatively aseismic regions (such as northern France or southwestern France away from the Pyrenees).

The time span shown in Fig. 1 is too short to characterize the distribution and expected maximum size of intraplate earthquakes properly. The largest intraplate earthquake since 1989 in Europe was the 1992 Roermond, Netherlands $M_w = 5.3$ event in the Lower Rhine embayment (Van Eck and Davenport 1994), which is small compared to the largest event shown on Fig. 1, the $M_w = 7.6$ 1999 Izmit, Turkey earthquake, but caused considerable losses of about US$150 Million (Berz 1994). Large intraplate earthquakes are rare but a repeat of the 1356 Basel, Switzerland earthquake, the largest historic earthquake north of the Alps, estimated as M_w 6.7–7.1 (Fäh et al. 2009), could cause billions of US$ in damage.

3 Data and Method

The bulk of the moment tensor solutions shown in this paper are obtained by regional moment tensor (RMT) inversion. The method is presented in Nabelek and Xia (1995) and has been successfully applied in the European-Mediterranean region (Braunmiller et al. 2002). I refer to the two papers for details of the method and its application. Long-period, three-component waveform modeling provides robust results for

the seismic moment tensor, seismic moment, and centroid depth. The method can be applied routinely to M_w 4.0–4.5 and larger earthquakes and in regions of dense broadband seismic networks (such as Switzerland and parts of Germany) to events as small as $M_w \approx 3.0$.

Regional broadband data were obtained from several international (IRIS, Geofon, Geoscope, ORFEUS) and national (Austria, Germany, Israel, and Switzerland) data centers. The network of broadband seismic stations in the European-Mediterranean region has expanded rapidly in the last 25 years and for an overview of currently openly available broadband stations visit the European Integrated Data Archive hosted by the ORFEUS data center (www.orfeus-eu.org). The stations available for this study are roughly similar to the station map shown in Braunmiller et al. (2002).

The RMT database covers the 1995–2007 period and includes the 1978 $M_w = 5.2$ Swabian Alb, Germany and other selected 1989–1994 events for which sufficient broadband data exist. Some solutions shown here have been published elsewhere (Braunmiller et al. 2002; Braunmiller 2002; Bernardi et al. 2005; and yearly reports of the Swiss Seismological Service: Baer et al. (2007) and references therein). The European intraplate and plate boundary zone events discussed here are a subset of the complete RMT database; its publication is in preparation.

4 Results

The database of European intraplate source parameters considers only events that are at least 125 km from an active plate boundary (defined by thick solid lines in Fig. 2). Analysis of regional data reduces the magnitude threshold compared to teleseismic methods. The database includes 451 RMT solutions (1995–2007: 433) compared to 225 Global CMT solutions (Dziewonski et al. 1981; Ekström et al. 2012) for 1976–2015, or 33 compared to fewer than 6 events per year. The 87 common events are compared (see Appendix) and high similarity of results attests to robustness and reliability of waveform modeling derived source parameters.

For further analysis, I excluded sub-crustal earthquakes (depth $z > 40$ km) associated with current subduction zones (Tyrrhenian Sea, Hellenic arc) and the slab remnant of the Carpathian arc resulting in 504 unique crustal seismic events. Strong events ($M \geq 3.5$) induced by mining and hydrocarbon extraction are relatively common in parts of Poland, Germany, the Netherlands, and in the North Sea and 29 such events are identified in Fig. 2; while not focus of this paper, it is noteworthy that their source parameters overall agree well with Cesca et al. (2013).

The color scheme in Fig. 2 and subsequent maps follows the World Stress Map project (www.world-stress-map.org) with red for normal faulting, green for strike-slip, blue for thrust faulting, and black for "unknown". The categories of the stress regime are defined by principal axes orientations and given in Zoback (1992). The results in terms of deformation style and orientation of the maximum horizontal stress direction S_{Hmax}, as expected, agree extremely well with the existing stress data shown for the European-Mediterranean region, e.g., in Heidbach et al. (2016). An

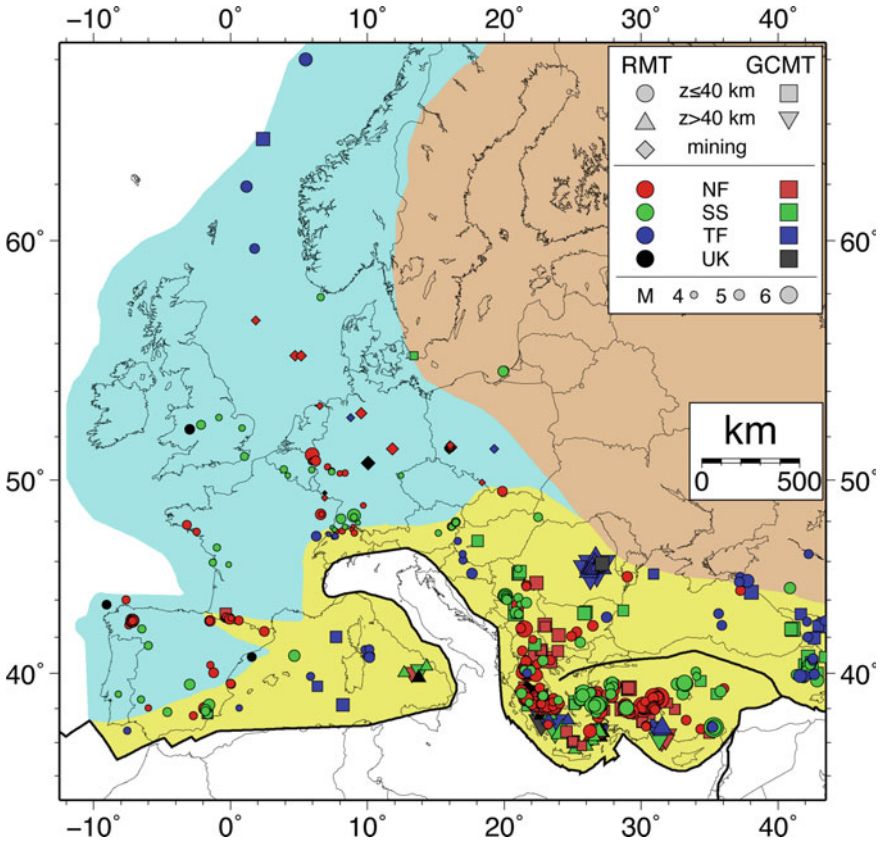

Fig. 2 Distribution of seismic events with regional moment tensor (RMT) and/or Global CMT solution in Europe. The 475 shallow crustal earthquakes are shown as circles (RMT) and squares (GCMT), respectively, and color-coded to indicate different stress regimes (following World Stress Map classification). Symbol size scales with M_w. The 29 suspected mining and hydrocarbon extraction events are marked as diamonds. In addition, 85 sub-crustal (z > 40 km) events are shown as triangles (RMT) and inverted triangles (GCMT), respectively, but are not discussed further. Otherwise as Fig. 1

important point, though, is that all source parameters shown here are derived from long-period waveform modeling and, as shown in Figs. 3 and 4, provide internally highly consistent results for different sub-regions.

4.1 Southeastern Europe, Anatolia and Caucasus

The focus of this contribution is on Western Europe and results for other areas are only summarized. Figure 3 shows fault plane solutions and S_{Hmax} directions for

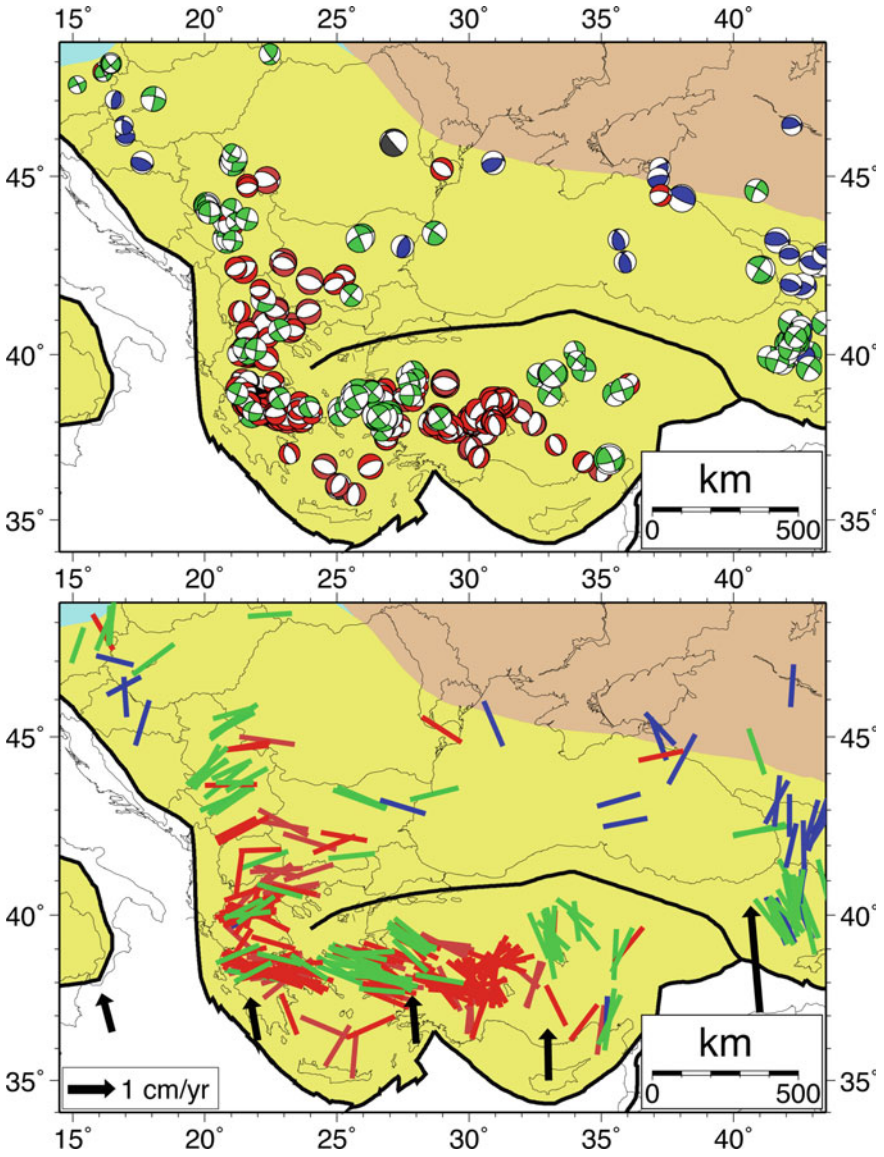

Fig. 3 Top: Fault plane solutions in southeast Europe, Anatolia and the Caucasus. Shown are 356 crustal events with depth z $\leq$ 40 km and a minimum double couple contribution of 20% to exclude mechanisms with ill-constrained principal axes. Event color-coding as in Fig. 2 and background color scheme as in Fig. 1. Note high consistency of mechanisms within regions. Plot order: "unknown", thrust, normal and strike-slip on top. Bottom: S_{Hmax} directions for same earthquakes ("unknown" excluded). Black arrows show MORVEL (DeMets et al. 2010) Nubia-Eurasia and Arabia-Eurasia plate motion vectors, respectively

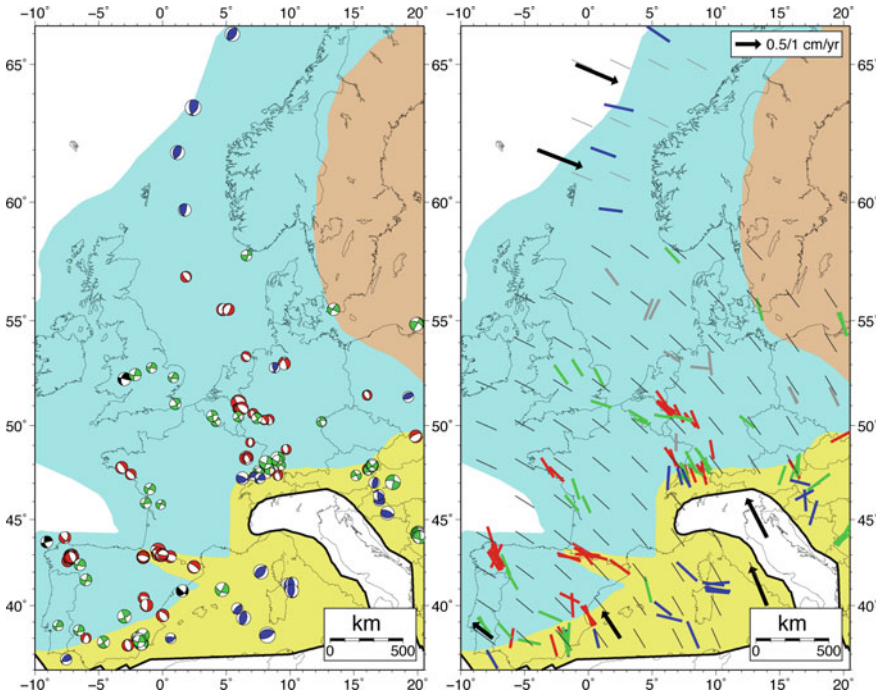

Fig. 4 Left: Fault plane solutions in Western Europe. Shown are 139 crustal seismic events ($z \leq 40$ km) with a minimum double couple and deviatoric moment tensor contribution of 20% and 60%, respectively, to exclude mechanisms with ill-constrained axes orientations. Non-deviatoric sources are considered only for the 29 mining or hydrocarbon-extraction related seismic events; 10 have a significant deviatoric contribution and are shown. Otherwise as Fig. 3. Right: S_{Hmax} directions for same earthquakes ("unknown" excluded and gray bars for non-tectonic events). Black arrows show MORVEL Nubia-Eurasia (scale is 0.5 cm/yr) and North America-Eurasia (scale is 1.0 cm/yr) plate motion vectors, respectively. Thin black lines are trajectories of MORVEL Nubia plate motion relative to Europe; thin gray lines (north of 60° N) show same for North America

events in southeastern Europe, Anatolia and the western Caucasus. The majority of events in the combined (RMT and GCMT) dataset occurred in the Aegean region and in western-central Anatolia in the back arc of the Hellenic and Cyprus arcs where Africa (Nubia) slowly subducts beneath the Aegean and Anatolian blocks.

In the Aegean Sea and western Anatolia region (about south of 39.5° N and west of 30° E), N-S extension and westward escape of Anatolia are accommodated by E-W striking normal faults and by right-lateral strike slip faulting; the S_{Hmax} direction is close to WNW-ESE (median: 105°; 153 events); within uncertainties (~21°), this is consistent with Müller et al. (1992). A few normal faulting mechanism in the southern Aegean Sea suggest arc parallel strikes of active normal faults in the southern Cyclades and southern Peloponnesus (three events near 37° N, 23°–26.5° E), which further south (~36° N) seems to give way to E-W extension in the overriding crust perpendicular to the arc consistent with observed GPS vectors (Hollenstein

et al. 2008). In northern Greece and the southwestern Balkans (about 39.5°–45° N), GPS velocities relative to Eurasia decrease (Hollenstein et al. 2008). The dominant deformation style changes from normal to strike-slip faulting going northward, and the S_{Hmax} direction, which is WSW-ENE (median: 76°; 92 events), is slightly rotated counterclockwise relative to the Aegean block.

The faulting style in central and eastern Anatolia (east of 30° E) in the back arc of the Cyprus trench changes from normal to predominantly strike-slip going towards the east. The S_{Hmax} direction, overall, is roughly N-S oriented (median: 183°; 47 events) but more variable than in the Aegean and western Anatolia region.

The Caucasus region is undergoing north-south contraction due to Eurasia-Arabia collision. Strike-slip mechanisms with NNW-SSE S_{Hmax} direction (median: 167°; 24 events) prevail in the Armenian Plateau (about 40° N). Further north, in the Greater Caucasus Mountains, deformation changes to thrust faulting and the S_{Hmax} direction rotates slightly to NNE-SSW (median: 13°; 11 events). Few stress indicators exist north of the Caucasus in the Precambrian shield region (e.g., Heidbach et al. 2016); results from a few focal mechanisms shown here indicate deformation may remain compressional with roughly N-S directed S_{Hmax}. Similarly, few stress data exist for the Black Sea; S_{Hmax} seems to be oriented roughly E-W within the Mesozoic domain and slightly more northerly near the Mesozoic-Precambrian boundary.

Focal mechanisms in the northwest part of Fig. 3 (about north of 45° N and west to 25° E) reflect deformation due to collision of the Adria microplate with Eurasia. GPS data (e.g., Grenerczy et al. 2005) indicate a few mm/yr NNE-directed motion, which is taken up over a broad region from the coast across the Dinarides and into the Pannonian basin. This is consistent with the thrust mechanisms with roughly NNE-SSW S_{Hmax} direction between 45°–47° N and left-lateral strike-slip motion further north reflecting eastward Alpine extrusion as suggested, e.g., by Grenerczy et al. (2005) and Grenerczy and Kenyeres (2006).

4.2 Northern and Western-Central Europe

Focal mechanisms and corresponding S_{Hmax} directions for intraplate earthquakes in northern and central-western Europe are shown in Fig. 4. I separate the events into three broad groups. The first consists of earthquakes in the Tyrrhenian Sea and the western Mediterranean Sea within the Mesozoic domain. Fault plane solutions in the western Mediterranean (west of the Tyrrhenian Sea) and south of Portugal show a mix of normal, strike-slip, and thrust faulting but have consistent NNW-SSE S_{Hmax} orientations, which is in broad agreement with the Nubia-Eurasia plate motion direction suggesting seismic activity is governed by plate interactions. The events probably reflect deformation in a broad plate boundary zone. The S_{Hmax} orientations are different at the western boundary (near 10° E) of the Tyrrhenian basin an extensional feature associated with the Apennine and Calabrian arcs (e.g., Malinverno 2012) where several N-S trending thrust mechanisms indicate E-W directed compression.

This suggests that stress conditions in the Tyrrhenian Sea might be dominated by local rather than larger-scale plate boundary forces.

The small second group consists of four thrust events between 59°–66° N along the continental margin offshore Norway. Their S_{Hmax} orientations are sub-parallel to the North America-Eurasia relative plate motion direction indicating the stress field is likely due to plate boundary forces ("ridge push") transmitted through the oceanic plate (e.g., Stein et al. 1989). A significant percentage of the larger SCR earthquakes globally are located at passive rifted margins (e.g., Johnston 1989). The largest SCR event ($M_w = 5.6$) during the last 40+ years in the study area is the margin earthquake near ~63° N (Fig. 4) and two additional margin events reached $M_w = 5$.

The third group includes events in the Precambrian (brown) and Paleozoic (blue, south of 59° N) domains, as well as events within ~50 km of the Mesozoic-Paleozoic domain boundary (Fig. 4). This group represents seismicity in stable continental crust (SCR) and includes 122 seismic events of which 29 are non-tectonic; of the 122 solutions, 120 are regional moment tensors. This group will be discussed below.

5 Discussion

The seismic events over the broad SCR region of western-central Europe show remarkably consistent source mechanisms and S_{Hmax} orientations. Away from the vicinity of the Alps in northwest Switzerland and excluding non-tectonic events, all focal mechanisms are either normal or strike-slip (Fig. 4 left). This is consistent with compilations of first motion focal mechanisms for Switzerland (Kastrup et al. 2004), the Rhine Graben area (Bonjer 1997; Plenefisch and Bonjer 1997), and the Armorican Massif and Massif Central regions of France (Nicolas et al. 1990; Delouis et al. 1993) that show predominance of normal and strike-slip faulting. Mechanisms within small sub-regions are generally similar (such as the western Pyrenees) and change smoothly (e.g., from normal faulting in Pyrenees to strike-slip and then back to normal faulting along the French Atlantic coast in the western Armorican Massif). In northwestern Switzerland and the southern Rhine Graben region (near 47° N and 8° E), RMTs show a range of deformation styles within a small source region consistent with, e.g., Kastrup et al. (2004) and the mechanisms agree well with first motion solutions from the dense Swiss seismic network (Baer et al. (2007) and references therein for comparison of 1999–2006 events).

The orientation of the maximum compressive horizontal stress S_{Hmax} in Western Europe is predominantly NW-SE directed (Fig. 4, right). The orientation changes systematically and remains roughly parallel to the relative motion of Nubia (Africa) with respect to the Eurasian plate. This suggests that plate boundary forces exerted by the Nubia-Eurasia collision are the primary control on the European intraplate stress field. The average S_{Hmax} orientation is 145° ± 26° (Fig. 5 left) and the S_{Hmax} orientations differ from the local trajectories of the Nubia-Eurasia plate motion by only 12° ± 26° (Fig. 5 right). As expected, the results are very similar to the World Stress Map estimates (Müller et al. 1992; Heidbach et al. 2007, 2016) and to formal

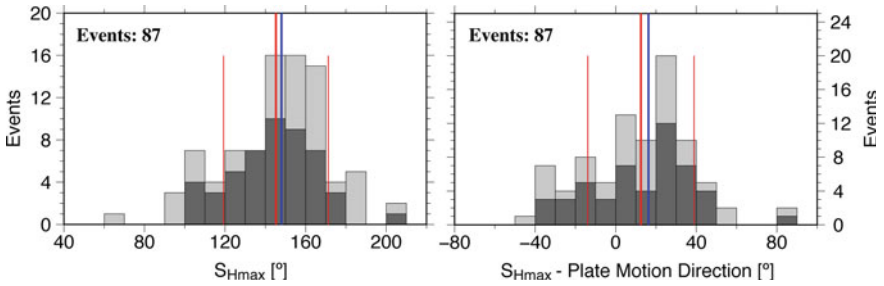

Fig. 5 Left: Histogram of S_{Hmax} orientations in central-western Europe for 87 (of 93) earthquakes with defined stress regime (following Zoback 1992) south of 59° N (Fig. 4). Light gray shows all events; dark gray only earthquakes in the Paleozoic domain. Average orientation is 145° (bold red line) with standard deviation of 26° (thin red lines); median value is 148° (bold blue line). Values for the Paleozoic domain only are 144° ± 21° and 146°, respectively. Right: Histogram of orientation differences between S_{Hmax} and the Nubia-Eurasia plate motion trajectory (calculated at the event location using MORVEL rotation pole). Gray and color scheme as on left. Average and median for all events are: 12° ± 26° and 16°, and for the Paleozoic domain only: 14° ± 25° and 18°

stress tensor inversions for central Europe north of the Alps (e.g., Plenefisch and Bonjer 1997; Kastrup et al. 2004).

Outliers in S_{Hmax} orientations (Fig. 5, left) are associated with anomalous events and almost all are located in the Mesozoic-Paleozoic boundary region (light gray shading in Fig. 5). A single Paleozoic outlier with $S_{Hmax} \geq 200°$ comes from an earthquake in northwestern Spain, which is part of a 1995–1998 sequence of 11 events where all other events have "normal" orientations between 146° and 171°. The second event with $S_{Hmax} \geq 200°$, and three others with $S_{Hmax} \geq 180°$, occurred in eastern Austria possibly related to eastward extrusion of the Eastern Alps and are thus not part of stable central-western Europe. The two other $S_{Hmax} \geq 180°$ events, one in the French Jura and one in southern Spain, are likely affected by stress perturbations caused by the Alps and Betic Mountains within the Nubia-Eurasia boundary zone, respectively.

The single $S_{Hmax} \approx 60°$ observation in Fig. 5 is from an unusual normal faulting earthquake in southern Poland (near 50° N) (Wiejacz and Debski 2009); it is not clear how the event's stress indicators relate to the rest of central-western Europe. It is interesting to note that S_{Hmax} from mining related events with significant deviatoric components in southwestern Poland (gray lines, Fig. 4) are consistent with earthquake observations in central-western Europe and with local Nubia-Eurasia plate motion trajectories. However, mining and hydrocarbon extraction related events often show significant S_{Hmax} deviations (e.g., northern Germany and Central Graben, North Sea) probably caused by local stress field perturbations.

The other three events with $S_{Hmax} \leq 100°$ are in the western Pyrenees, where a group of 8 events with a median $S_{Hmax} = 107°$ indicates a counterclockwise rotation of the stress field relative to the Nubia-Eurasia direction that could be due to a crustal root as suggested for the Alps (Kastrup et al. 2004). Most outliers come

from the Mesozoic-Paleozoic boundary region suggesting larger local stress field variations occur in the more mobile Mesozoic domain. Without the outliers, the S_{Hmax} distribution tightens to a ~100°–170° range similar to the World Stress Map data (e.g., Müller et al. 1992). A certain amount of S_{Hmax} spread is expected because earthquakes usually occur on pre-existing faults that rupture under the prevailing stress field even if a fault is not optimally aligned leading to differences between expected and actual S_{Hmax} directions.

The region north of the Alps to the Lower Rhine Embayment (Fig. 6) is one of the most seismically active regions in central Europe and the RMT dataset includes the strong 1978 Swabian Jura, Germany (M_w = 5.2) and 1992 Roermond, Netherlands (M_w = 5.3) earthquakes. Like Plenefisch and Bonjer (1997), I find the S_{Hmax} direction rotates by about 30° counterclockwise from the northern Alpine Foreland and broader Southern Rhine Graben region south of 49° N (median: 159°) to events in the Lower Rhine Embayment and Ardennes Massif north of 50° N (median: 130°). The rotation is possibly due to a regional stress field perturbation caused by the lateral density contrast of a crustal root beneath the Alps as proposed by Kastrup et al. (2004) for the Alps proper.

Subdividing events south of 49° N according to latitude or depth does not reveal significant differences between a northern and southern group, or between shallow and deeper events, respectively. The deformation regime, however, changes with depth as strike-slip events dominate in the upper crust (z < 15 km) while normal faulting events are more common at depth z > 15 km (Plenefisch and Bonjer 1997).

Figure 7 (left) shows the earthquake depth distribution for western-central Europe. Only events with well-constrained RMT depth are shown and considering their size (Fig. 7 right), centroids obtained from long-period waveforms are equivalent to hypocenters. Earthquakes are observed throughout most of the crust from about 0–30 km depth. Most events occur at 10–15 km depth but shallow events (z < 10 km) are common while activity overall decays with depth from 15 to 30 km. The small, but well-constrained dataset does not support the idea of a bimodal distribution of SCR event depth (cf. Klose and Seeber 2007).

Consistent with earlier observations of lower crustal earthquakes east of the Southern Rhine Graben and beneath the Alpine Foreland (e.g., Deichmann 1992; Bonjer 1997), I find 8 of 13 events south of 48° N (Fig. 6) at mid-to-lower crustal depths of 18-27 km. Brittle failure in the lower crust probably requires the presence of fluids (Deichmann 1992).

Earthquakes in the Lower Rhine Embayment (Fig. 6) occur primarily from shallow-to-mid crustal depths of ~4–20 km (Reamer and Hinzen 2004). The RMT database includes 4 km shallow events associated with the 2001 Voerendaal, Netherlands swarm (Goutbeek and Dost 2004) but the largest events (1992 M_w = 5.3 Roermond and 2002 M_w = 4.6 Alsdorf, Germany) seem to be concentrated at 15–18 km close to the bottom of the seismogenic zone; these depths are consistent with travel-time based locations and other modeling (e.g., Van Eck and Davenport 1994 and references therein; Braunmiller et al. 1994; Hinzen and Reamer 2007).

A main advantage of using regional waveform data is that smaller seismic events can be analyzed. Large earthquakes that can be analyzed with teleseismic data occur

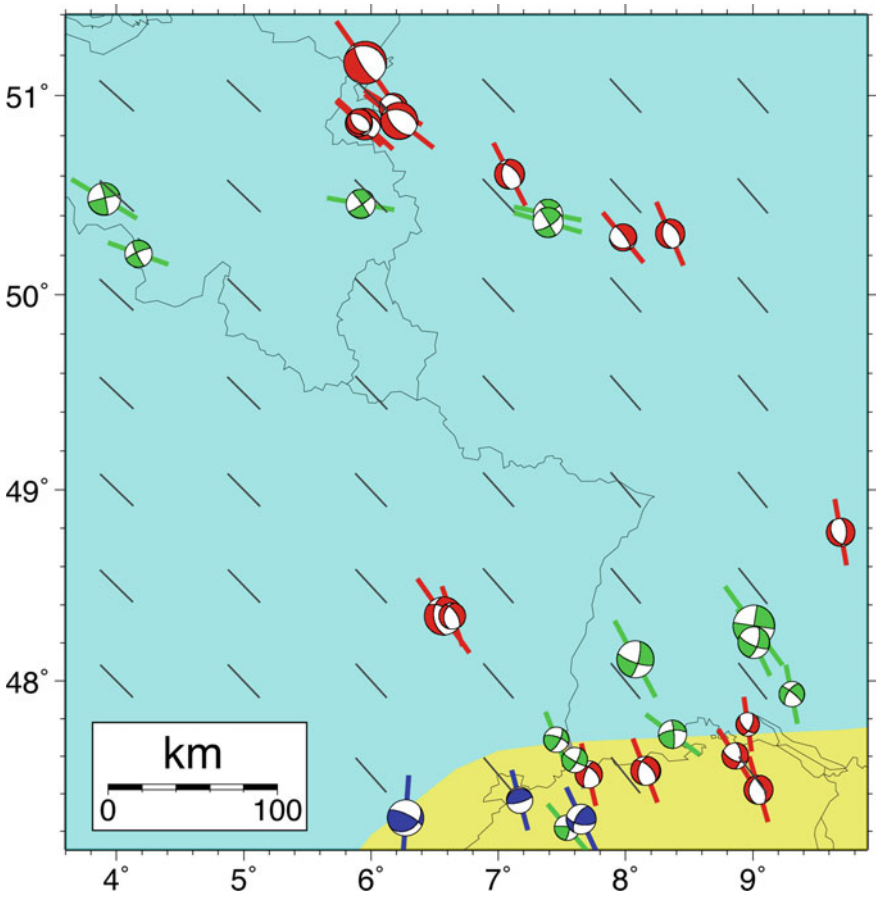

Fig. 6 Close-up from northern Alpine foreland to Lower Rhine Embayment with fault plane solutions, S_{Hmax} orientations, and Nubia-Eurasia motion trajectories. Symbols and colors as in Fig. 4. Note south to north counterclockwise S_{Hmax} rotation. Mining related event near 49° N (Fig. 4) is omitted

rarely in SCRs making it difficult to study SCR seismic behavior. The 40-year GCMT catalog (1976–2015) contains 13 SCR events in central-western and northern Europe (events away from yellow "Mesozoic" region of Fig. 4) compared to 94 earthquakes in the RMT database. Figure 7 (right) shows the size distribution of the combined set (94 RMTs plus 3 unique GCMTs). The dark gray shading shows 85 RMTs for 1995–2007 for which the number of solutions increases down to M_w =4.2–4.3 providing a rough estimate for RMT catalog completeness. More than half of the RMTs are $M_w < 4.2$ from events in regions with relatively dense broadband seismic networks already during 1995–2007. The threshold is probably lower now. The recent and ongoing expansion of broadband networks in Europe and elsewhere provides an unprecedented opportunity to obtain reliable earthquake source parameters for stable

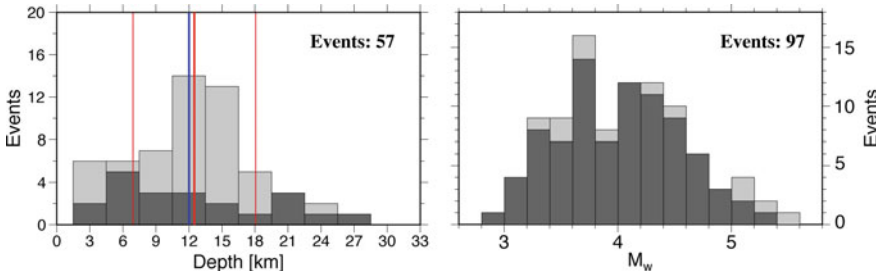

Fig. 7 Left: Centroid depths from RMT analysis in central-western Europe for 57 earthquakes with well-constrained depth (variance increase ≥5% for depth change of up to ±10 km). Light gray are all events, dark gray only earthquakes in the Paleozoic-Mesozoic boundary domain to highlight the Alpine Foreland where most of the deeper events occurred. Average depth: 12.5 ± 5.6 km (red), median: 12 km (blue). Right: Size distribution of 97 earthquakes (mining events excluded) in Precambrian, Paleozoic, and Paleozoic-Mesozoic boundary domains of Fig. 4; 94 RMTs and 3 GCMTs (events with no RMT). Dark gray are 85 RMTs for 1995–2007 when station distribution allowed systematic analysis of entire region

continental regions globally from regional waveform analysis with direct applications such as to the World Stress Map project (Heidbach et al. 2007) and to gain understanding of seismogenesis in stable continental regions and other intraplate settings towards improving hazard assessments (e.g., Johnston et al. 1994; Stein and Mazzotti 2007).

6 Conclusions

Analysis of regional broadband seismic data significantly increases the European source parameter database (moment tensor, depth, M_w, S_{Hmax}) for intraplate earthquakes and earthquakes within plate boundary deformation zones compared to teleseismic analysis. The combined set of 504 unique crustal seismic events within Europe and at least 125 km away from an active plate boundary includes 390 RMT solutions, primarily for 1995–2007, and 114 GCMT solutions for 1976–2015.

Most solutions (378) are from earthquakes in the broadly deforming plate boundary zones associated with the Nubia-Eurasia subduction in the western Mediterranean and the Aegean and Anatolian backarc extension and deformation regions, as well as with Arabia-Eurasia collision in the Caucasus. Deformation styles and orientations of the maximum horizontal compressive stress direction S_{Hmax} are consistent with earlier findings and indicate a dominance of plate boundary forces on deformation and stress orientations in actively deforming regions.

For the stable continental regions of northern and central-western Europe, the 123 RMT solutions constitute the bulk of available source parameters (total: 126—plus 10 "doubles" see Appendix) derived from stable, reliable long-period three-component waveform modeling. Earthquakes near the continental margin offshore Norway have

thrust mechanisms with roughly E-W oriented S_{Hmax} orientations sub-parallel to the North America-Eurasia plate motion direction indicating that "ridge-push" plate boundary forces control the stress field and deformation; the largest ($M_w = 5.6$) SCR event in Europe since 1976 is part of this small 4-event group.

The average S_{Hmax} orientation in the SCR of central-western Europe is $145° \pm 26°$ consistent with World Stress Map observations and formal stress tensor inversions of compilations of first motion fault plane solutions. The S_{Hmax} orientation is sub-parallel to the Nubia-Eurasia plate motion direction (average deviation is $12° \pm 26°$) indicating that Nubia-Eurasia plate boundary forces control the large-scale stress field in stable Europe. Local deviations observed in the Pyrenees and in the northern Alpine Foreland are probably due to stress field perturbations caused by the crustal roots of the mountain ranges. Event depths do not show a general bi-modal depth distribution in the European SCR. However, earthquake depths in the northern Alpine Foreland reach into the lower crust (to ~30 km) and likely require the presence of fluids to allow brittle deformation. In the Lower Rhine Embayment, earthquakes are slightly shallower (to ~20+ km) but the largest recent events seem to concentrate towards the bottom of the seismogenic zone ($\geq$15 km).

Regional waveforms allow systematic source parameter retrieval of earthquakes that are significantly smaller than events that can be analyzed with teleseismic data. In regions of low seismicity and infrequent larger events, such as most SCRs and intraplate regions, deformation style, event depth, and stress orientations can be estimated from the more frequent moderate-sized earthquakes ($M_w \geq 3.5$ depending on broadband seismic network density) through regional moment tensor inversion.

Appendix

Of the earthquake shown in Fig. 2, including the sub-crustal events with depth $z > 40$ km, 87 have a RMT and a Global CMT solution. This appendix compares results from the two methods to illustrate overall robustness and reliability of waveform modeling derived source parameter estimates.

Figure 8 shows the double couple (DC) fault plane solutions for the common events. With few exceptions, the agreement between the RMT (black and white) and GCMT (gray) solutions is high. Most events with large focal mechanism differences occurred before 2004 when GCMT analysis started to include intermediate-period surface waves (Ekström et al. 2012), which lowered GCMT analysis threshold and stabilized results for $M \approx 5$ and smaller events common in the European intraplate dataset. Expansion of broadband seismic networks in the European-Mediterranean region also improved RMT solution quality.

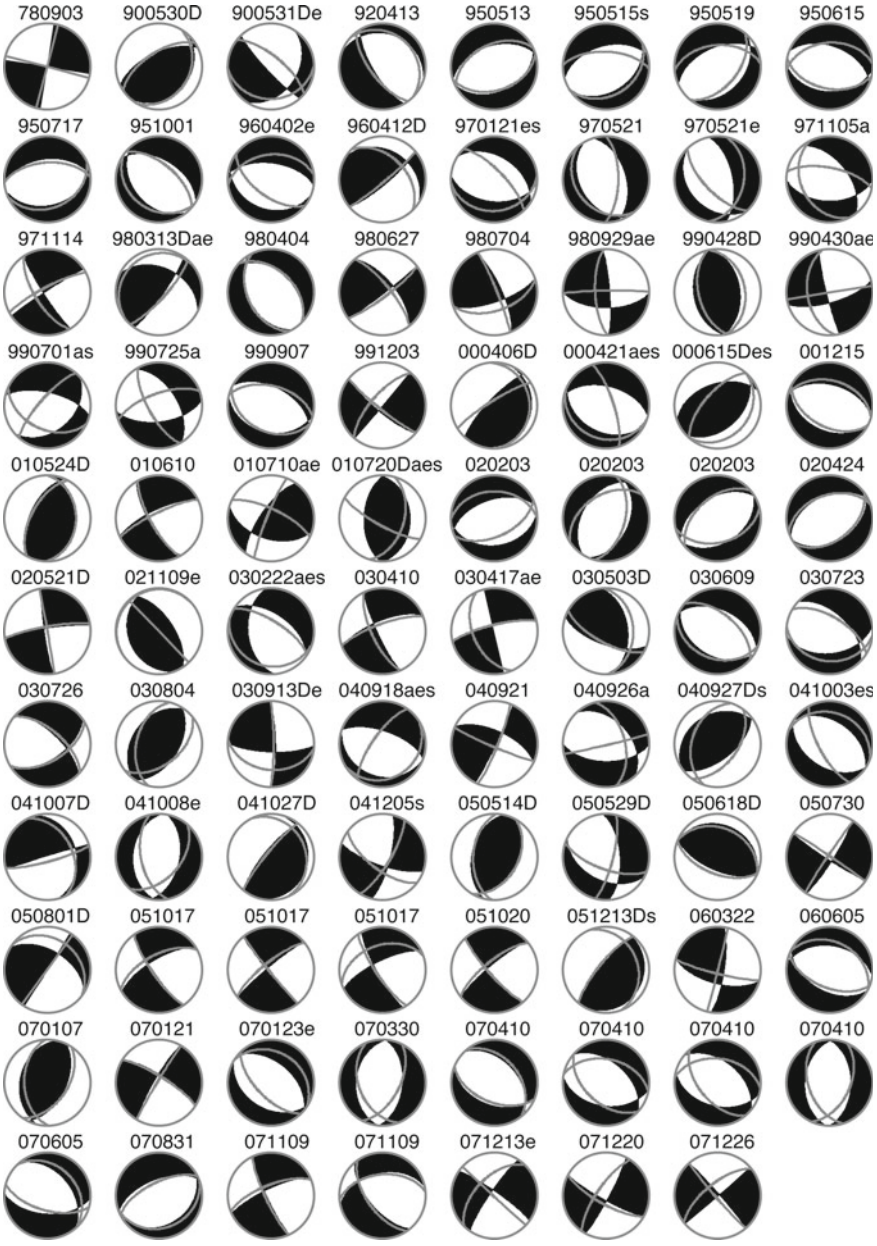
780903
900530D
900531De
920413
950513
950515s
950519
950615
950717
951001
960402e
960412D
970121es
970521
970521e
971105a
971114
980313Dae
980404
980627
980704
980929ae
990428D
990430ae
990701as
990725a
990907
991203
000406D
000421aes
000615Des
001215
010524D
010610
010710ae
010720Daes
020203
020203
020203
020424
020521D
021109e
030222aes
030410
030417ae
030503D
030609
030723
030726
030804
030913De
040918aes
040921
040926a
040927Ds
041003es
041007D
041008e
041027D
041205s
050514D
050529D
050618D
050730
050801D
051017
051017
051017
051020
051213Ds
060322
060605
070107
070121
070123e
070330
070410
070410
070410
070410
070605
070831
071109
071109
071213e
071220
071226

◀**Fig. 8** Fault plane solutions for 87 common RMT (black and white) and GCMT (gray lines) earthquakes in Europe. Numbers on top are year, month, and day of occurrence; events are in chronological order. Additional labels are "D": 20 sub-crustal events (z > 40 km); "a": 13 events with $|\Delta Ax| \geq 30°$; "e": 20 events with $\eta_p \leq 0.8$; and "s": 12 events with S_{Hmax} difference $\Delta S_{Hmax} \geq 15°$ (see text for explanation of $|\Delta Ax|$ and η_p). Four events labeled "aes" indicate large mechanism differences, they are: **A**. Event 000421 in western Anatolia, which is characterized by N-S extension; nearby events (970121, 030723, 030726) are consistent with the RMT solution. **B**. Event 010720 is one of the common intermediate-depth Vrancea, Romania events; the closest other events (050618, 051213) show high similarity. **C**. Event 030222 in eastern France is tightly constrained by regional waveforms (Deichmann et al. 2004); the event predates inclusion of intermediate-period surface waves and with $M_w = 4.8$ is small for traditional GCMT analysis. **D**. The GCMT solution for event 040918 in the Pyrenees has a 6% double-couple contribution and its orientation differs significantly from other nearby and internally consistent events in the RMTs database

The overall agreement is further illustrated in Fig. 9, which shows different measures of moment tensor similarity plotted against each other. The Kagan angle (Kagan 2007) is the minimum 3-D angle required to rotate the principal axes of one moment tensor onto another ('angular difference' between two double couples), $|\Delta Ax|$ is the mean angular difference between principal axes (Bernardi et al. 2004), which is a similar quantity as the Kagan angle and simple to calculate, and η_p is the radiation pattern coefficient (Kuge and Kawakatsu 1993), which describes the P-wave radiation pattern similarity between two moment tensors. Small values of $|\Delta Ax|$ and the Kagan angle, and large values of η_p indicate similar solutions. The roughly linear relation between $|\Delta Ax|$ and the Kagan angle is expected since both describe principal axes rotations. A strong correlation exists only for events with small Kagan angle and large η_p. About 74% of the events (64 of 87) satisfy high similarity criteria $|\Delta Ax| \leq 30°$ and $\eta_p \geq 0.8$ while the rest shows moderate similarity. Low DC percentages in moment tensors, shown as dark circles, account for a disproportional number of events with moderate similarity (23%) compared to their frequency of occurrence (14%). In contrast, all 22 events with high DC source contributions, shown as open circles, have low rotation angles and 86% of them satisfy high similarity criteria. Low DC percentages in RMT and GCMT solutions might thus, in many cases, indicate limited source parameter resolution rather than actual deviations from a simple faulting source.

The RMT and GCMT moment magnitudes agree very well with each other (Fig. 10 left). The average difference is 0.00 ± 0.11. The data indicate a slight tendency of M_w(GCMT) > M_w(RMT) for small events and vice versa for large events with linear regression resulting in a slope of 1.08. Figure 10 (right) shows centroid depths of all events in light gray. For shallow events, GCMT depth is often fixed while for deep events, depth is sometimes not well resolved by long-period regional data. The subset of dark gray circles consists of events with free (GCMT) and resolved (RMT) depth. For these 35 events, the average depth difference GCMT-RMT is 2.8 ± 10.1 km, and, for 19 crustal events ($z \leq 40$ km) is 1.3 ± 3.4 km indicating excellent agreement considering that RMT depth analysis is performed as grid search with 3 km steps.

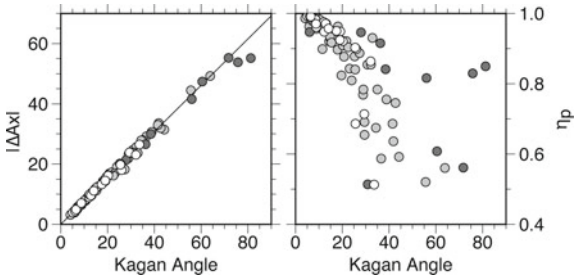

Fig. 9 Comparison between RMT and GCMT solutions. Kagan angle and |ΔAx| measure angular difference between principal axes systems while η_p measures P-wave radiation pattern similarity (normalized to [−1, 1]). An interchange of two axes results in |ΔAx| = 60°. Left: Kagan angle versus |ΔAx|. Dark circles indicate solutions with double-couple percentage of DC ≤ 35% in either RMT or GCMT; these solutions on average show larger differences. Open circles are events with DC ≥ 85% in both RMT and GCMT; all have |ΔAx| ≤ 30°, which Bernardi et al. (2004) considered to indicate high similarity. Gray circles are all other events. Kagan angle and |ΔAx| roughly show a 4/3 scaling (solid line) Right: Kagan angle versus η_p. Symbols are as on left. High correlation exists only for low Kagan angle and high η_p events (upper left of diagram); the larger scatter at lower similarities reflects that the two indicators measure separate aspects of radiation differences

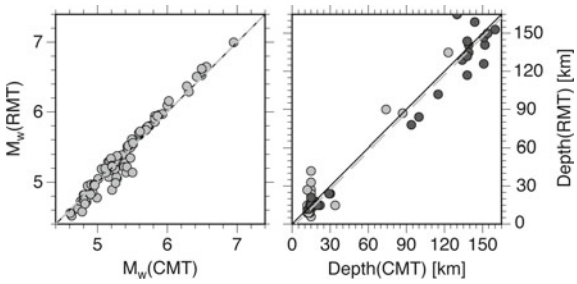

Fig. 10 Left: Comparison of M_w(GCMT) and M_w(RMT). Solid black line is a 1:1 relation and gray dashed line shows the average difference (0.00 ± 0.11). Right: Comparison of GCMT and RMT centroid depth. Light gray shows all 87 events. Dark gray shows 35 events with free (GCMT) and resolved (RMT) depth; their average difference, shown as gray dashed line, is 2.8 ± 10.1 km and for crustal events (z ≤ 40 km) is 1.3 ± 3.4 km

A histogram of the differences in the maximum horizontal stress orientation S_{Hmax} is shown in Fig. 11. Excluding low DC events (≤20% for either GCMT or RMT) and events with "unknown" stress regime (using Zoback (1992) assignments) results in 70 events. The average difference between RMT and GCMT is −0.7° ± 10.2°, while the median is −1° with 75% of all observations between −7° and 9° indicating S_{Hmax} orientations are stable and well resolved. The three outliers in Fig. 11 correspond to the suspicious 000421 (−48°), 030222 (24°), and 010720 (28°) events discussed

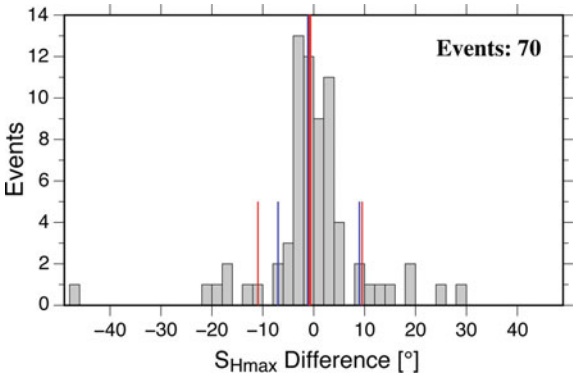

Fig. 11 Histogram of S_{Hmax} differences between RMT and GCMT solutions. Events with low DC (≤20%) or of "unknown" stress regime are excluded resulting in 70 common events. Red lines show average and standard deviation (−0.7° ± 10.2°) and blue lines median (−1°) and range containing 75% of observations (−7°–9°) indicating a tight distribution

in the context of Fig. 8 and should be disregarded. This leaves a remarkably small largest difference of −22° (normal faulting event 041003 at northwestern edge of Black Sea).

References

Baer M, Deichmann N, Braunmiller J et al (2007) Earthquakes in Switzerland and surrounding regions during 2006. Swiss J Geosci 100:517–528. https://doi.org/10.1007/s00015-007-1242-0

Bernardi F, Braunmiller J, Giardini D (2005) Seismic moment from regional surface-wave amplitudes: applications to digital and analog seismograms. Bull Seismol Soc Am 95(2):408–418. https://doi.org/10.1785/0120040048

Bernardi F, Braunmiller J, Kradolfer U et al (2004) Automatic regional moment tensor inversion in the European-Mediterranean region. Geophys J Int 157:703–716. https://doi.org/10.1111/j.1365-246X.2004.02215.x

Berz G (1994) Assessment of the losses caused by the 1992 Roermond earthquake, the Netherlands (extended abstract). In: van Eck T, Davenport CA (eds) Seismotectonics and seismic hazard in the Roer Valley graben; with emphasis on the Roermond earthquake of April 13, 1993. Geologie en Mijnbouw 73(2–4):281

Bonjer K-P (1997) Seismicity pattern and style of seismic faulting at the eastern border fault of the southern Rhine Graben. Tectonophysics 275:41–69

Braunmiller J (2002) Moment tensor solutions of stronger earthquakes in Germany with GRSN data. In: Korn M (ed) Ten years of german regional seismic network (GRSN). DFG Senate Commission for Geosciences, Report 25, pp 227–235

Braunmiller J, Kradolfer U, Baer M et al (2002) Regional moment tensor determination in the European-Mediterranean area—initial results. Tectonophysics 356(22):5–22

Braunmiller J, Dahm T, Bonjer K-P (1994) Source mechanism of the 1992 Roermond earthquake from surface-wave inversion of regional data. Geophys J Int 116:663–672

Cesca S, Rohr A, Dahm T (2013) Discrimination of induced seismicity by full moment tensor inversion and decomposition. J Seismol 17:147–163. https://doi.org/10.1007/s10950-012-9305-8

Coffin MF, Gahagan LM, Lawver LA (1998) Present-day plate boundary digital compilation. UTIG Technical Report No. 174, Progress Report No. 204-0598

Deichmann N (1992) Structural and rheological implications of lower-crustal earthquakes below northern Switzerland. Phys Earth Plant Int 69:270–280

Deichmann N, Baer M, Braunmiller J et al (2004) Earthquakes in Switzerland and surrounding regions during 2003. Eclogae Geol Helv 97:447–458

Delouis B, Haessler H, Cisternas A et al (1993) Stress tensor determination in France and neighboring regions. Tectonophysics 22:413–438

DeMets C, Gordon RG, Argus DF (2010) Geologically current plate motions. Geophys J Int 181:1–80. https://doi.org/10.1111/j.1365-246X.2009.04491.x

Dziewonski AM, Chou T-A, Woodhouse JH (1981) Determination of earthquake source parameters from waveform data for studies of global and regional seismicity. J Geophys Res 86:2825–2852. https://doi.org/10.1029/JB086iB04p02825

Ekström G, Nettles M, Dziewonski AM (2012) The global CMT project 2004–2010: centroid moment tensors for 13,017 earthquakes. Phys Earth Planet Inter 200–201:1–9

Fäh D, Gisler M, Jaggi B et al (2009) The 1356 Basel earthquake: an interdisciplinary revision. Geophys J Int 178:351–374

Goutbeek FH, Dost B (2004) First results on the analysis of the Voerendaal, the Netherlands, earthquake swarm of 2000–2002. In: Paper presented at the 29th general assembly of the European seismological commission, Potsdam, 2004

Grenerczy G, Kenyeres A (2006) Crustal deformation between Adria and the European platform from space geodesy. In: Pinter N et al (eds) The Adria microplate: GPS geodesy, tectonics and hazards. Springer, pp 321–334

Grenerczy G, Sella G, Stein S et al (2005) Tectonic implications of the GPS velocity field in the northern Adriatic region. Geophys Res Lett 32:L16311. https://doi.org/10.1029/2005GL022947

Heidbach O, Custodio S, Kingdon A et al (2016) Stress map of the Mediterranean and central Europe 2016. GFZ data service. https://doi.org/10.5880/WSM.Europe2016

Heidbach O, Reinecker J, Tingay M et al (2007) Plate boundary forces are not enough: second- and third-order stress patterns highlighted in the world stress map database. Tectonics 26:TC6014. https://doi.org/10.1029/2007tc002133

Hinzen K-G, Reamer SK (2007) Seismicity, seismotectonics, and seismic hazard in the northern Rhine area. In: Stein S, Mazzotti S (eds) Continental intraplate earthquakes: science, hazard, and policy issues. Geological Society of America Special Paper 425, pp 225–242. https://doi.org/10.1130/2007.2425(15)

Hollenstein C, Müller MD, Geiger A et al (2008) Crustal motion and deformation in Greece from a decade of GPS measurements, 1993–2003. Tectonophysics 449:17–40. https://doi.org/10.1016/j.tecto.2007.12.006

Johnston AC (1996) Seismic moment assessment of earthquakes in stable continental regions—III. New Madrid 1811–1812, Charleston, 1886 and Lisbon, 1755. Geophys J Int 126:314–344

Johnston AC (1989) The seismicity of 'stable continental interiors'. In: Gregersen S, Basham PW (eds) Earthquakes at North-Atlantic passive margins: neotectonics and postglacial rebound. Kluwer Academic Press, pp 299–327

Johnston AC, Coppersmith KJ, Kanter LR et al (1994) The earthquakes of stable continental regions: assessment of large earthquake potential. In: Schneider JF (ed) TR-102261, vol 1–5, Electric Power Research Institute (EPRI), Palo Alto, CA

Kagan YY (2007) Simplified algorithm for calculating double-couple rotation. Geophys J Int 171:411–418. https://doi.org/10.1111/j.1365-246X-2007.03538.x

Kastrup U, Zoback ML, Deichmann N et al (2004) Stress field variations in the Swiss Alps and the northern Alpine foreland derived from inversion of fault plane solutions. J Geophys Res 109:B01402. https://doi.org/10.1029/2003JB002550

Klose CD, Seeber L (2007) Shallow seismicity in stable continental regions. Seismol Res Lett 78(5):554–562

Kuge K, Kawakatsu H (1993) Significant non-double couple source components in deep and intermediate-depth earthquakes: Implications from moment tensor inversion of long-period seismic waves. Phys Earth Planet Inter 75:243–266

Malinverno A (2012) Evolution of the Tyrrhenian Sea-Calabria Arc system: the past and the present. Rend Online Soc Geol It 21:11–15

Müller B, Zoback ML, Fuchs K et al (1992) Regional patterns of tectonic stress in Europe. J Geophys Res 97(B8):11,783–11,803

Nabelek J, Xia G (1995) Moment-tensor analysis using regional data: application to the 25 March, 1993, Scotts Mills, Oregon earthquake. Geophys Res Lett 22:13–16

Nicolas M, Santoire JP, Delpech PY (1990) Intraplate seismicity: new seismotectonic data in Western Europe. Tectonophysics 179:27–53

Plenefisch T, Bonjer K-P (1997) The stress field in the Rhine Graben area inferred from earthquake focal mechanisms and estimation of frictional parameters. Tectonophysics 275:71–97

Reamer SK, Hinzen K-G (2004) An earthquake catalog for the Northern Rhine area, central Europe (1975–2002). Seismol Res Lett 75(6):713–725

Stein S, Mazzotti S (eds) (2007) Continental intraplate earthquakes: science, hazard, and policy issues. Geological Society of America Special Paper 425

Stein S, Cloetingh S, Sleep NH et al (1989) Passive margin earthquakes, stresses and rheology. In: Gregersen S, Basham PW (eds) Earthquakes at North-Atlantic passive margins: neotectonics and postglacial rebound. Kluwer Academic Press, pp 231–259

Talwani P (ed) (2014) Intraplate earthquakes. Cambridge University Press

Van Eck T, Davenport CA (1994) Seismotectonics and seismic hazard in the Roer Valley Graben; with emphasis on the Roermond earthquake of April 13, 1992. Geologie en Mijnbouw 73(2–4):91–92

Wiejacz P, Debski W (2009) Podhale, Poland earthquake of November 30, 2004. Acta Geophys 57:346–366. https://doi.org/10.2478/s11600-009-0007-8

Zoback ML (1992) First- and second-order patterns of stress in the lithosphere: the world stress map project. J Geophys Res 97:11,703–11,728